Tellus
SERIES A
DYNAMIC
METEOROLOGY
AND OCEANOGRAPHY
PUBLISHED BY THE INTERNATIONAL METEOROLOGICAL INSTITUTE IN STOCKHOLM

Tellus (2008), 60A, 885–897
Printed in Singapore. All rights reserved

TELLUS

Barrier layers and tropical Atlantic SST biases in coupled GCMs

By W.-P. BREUGEM[1,5], P. CHANG[2*], C. J. JANG[2,3], J. MIGNOT[4] and W. HAZELEGER[1],
[1]*Royal Netherlands Meteorological Institute (KNMI), De Bilt, The Netherlands;* [2]*Department of Oceanography, Texas A&M University, College Station, TX 77843, USA;* [3]*Korea Ocean Research & Development Institute (KORDI), Ansan, Republic of Korea;* [4]*LOCEAN, Université Pierre et Marie Curie, Paris, France;* [5]*Laboratory for Aero and Hydrodynamics, Delft University of Technology, Delft, The Netherlands*

(Manuscript received 13 September 2007; in final form 13 May 2008)

ABSTRACT

Barrier layers (BLs) tend to suppress entrainment cooling of the ocean surface mixed layer. Consequently, model biases in BL formation may result in SST biases. Coupled General Circulation Models (GCMs) capture the major observed BL regions in the tropical Atlantic, although with considerable biases in the BL characteristics. Thick BLs form in the Northwestern Tropical Atlantic (NwTA) during boreal fall and winter. The effect of BL biases in the NwTA on the cold SST bias in this region is likely small. On the contrary, the models simulate spurious BLs in the Southeastern Equatorial Atlantic (SeEA), which contribute significantly to the warm SST bias in this region. These spurious BLs originate partly from a fresh surface bias associated with a southeastward displaced ITCZ and partly from a warm subsurface bias associated with the underestimated equatorial trades during boreal spring and summer. It is hypothesized that a positive BL–SST–ITCZ feedback mechanism exists by which the BL and SST biases in the SeEA are maintained. An implication is that the upper ocean salinity stratification is a significant link in the chain of cause and effect by which precipitation and wind stress biases already present in uncoupled atmospheric models are amplified in coupled models.

1. Introduction

The ocean mixed-layer is the turbulent surface layer of the ocean with a vertically uniform density, temperature and salinity distribution. In the tropics, the base of the mixed layer corresponds to the top of the pycnocline. Over most of the tropical oceans the pycnocline coincides with the thermocline, but in regions with a strong vertical salinity stratification the pycnocline can be shallower than the thermocline. In this case, the layer between the top of the pycnocline and the top of the thermocline is called 'barrier layer (BL)' (Godfrey and Lindstrom, 1989; Sprintall and Tomczak, 1992), because it forms a barrier to entrainment and turbulent mixing of cold thermocline water into the mixed layer and inhibits the downward mixing of momentum (e.g. Vialard and Delecluse, 1998a). BLs thus have an impact on the SST and the surface currents (Murtugudde and Busalacchi, 1998; Maes et al., 2002).

Observational studies show that BLs can occur over the western and equatorial tropical Atlantic (Sprintall and Tomczak, 1992; Pailler et al., 1999; Foltz et al., 2004; Sato et al., 2006; de Boyer Montégut et al., 2007; Mignot et al., 2007). Advection of fresh water from the Amazon river by surface currents along the northern coast of South America induces thick BLs in this area in boreal winter and spring (Pailler et al., 1999; Masson and Delecluse, 2001). In summer, the North Equatorial Counter Current (NECC) carries part of the fresh Amazon water eastward across the basin, which reinforces the BLs induced by intense local precipitation in the ITCZ (e.g. Pailler et al., 1999). The tropical Atlantic is also characterized by robust BLs located equatorward of the subtropical salinity maxima during the winter season of both hemispheres. Their formation mechanism is still under debate (Sato et al., 2006; Mignot et al., 2007). Finally, Mignot et al. (2007) underlined the presence of up to ~50 m thick BLs east of the Caribbean basin and north of South America in boreal fall and winter. These BLs are characterized by a subsurface temperature inversion of which the maximum temperature is typically ~0.5–0.6°C higher than the mixed-layer temperature (de Boyer Montégut et al., 2007). They are probably formed by advection of fresh water from the Amazon river by surface currents in combination with surface cooling during boreal fall and winter (Mignot et al., 2007).

Many of the modelling studies on BL dynamics have been focused on the warm pool region in the western Pacific (e.g. Vialard and Delecluse, 1998a,b; Maes et al., 2002). Masson

*Corresponding author.
e-mail: ping@tamu.edu
DOI: 10.1111/j.1600-0870.2008.00343.x

and Delecluse (2001) were the first to use an ocean GCM to study the formation of BLs in the Atlantic warm pool region. The use of an ocean-only model excludes interactions between the ocean and the atmosphere, which are known to be strong in the tropics, making it difficult to address issues concerning the climatic impact of BLs (Murtugudde and Busalacchi, 1998; Maes et al., 2002). The present study attempts to investigate the climatic circumstances and impact of BLs in the tropical Atlantic by analysing fully coupled ocean–atmosphere GCM simulations.

Breugem et al. (2006) recently diagnosed systematic biases of nine coupled GCMs in simulating the tropical Atlantic climate. Biases that are common to all the models include a warm SST bias over the Southeastern Equatorial Atlantic (SeEA), especially in boreal summer, and a cold SST bias over the Northwestern Tropical Atlantic (NwTA). As a result, in boreal summer the zonal SST gradient along the equator is directed towards the east in the models instead of towards the west in the observations. For the same season, the simulated easterly trade winds along the equator are too weak. Similar biases were reported on the previous generation of coupled models (Davey et al., 2002). Furthermore, the simulated marine ITCZ with the associated band of deep convection and intense precipitation migrates too far southward into the southern hemisphere—a bias that is also typical for uncoupled atmospheric GCMs forced with observed SST (Biasutti et al., 2006).

One of the particularly pronounced characteristics of the models is the failure to accurately simulate the development of the equatorial Atlantic Cold Tongue (ACT) when the SST in the SeEA drops by about 6°C from late boreal spring to summer. In reality, the ACT develops as a result of increased entrainment and turbulent mixing of cold subsurface water into the mixed layer (Foltz et al., 2003). These processes are associated with the onset of the West African monsoon in May-June with the intensification of southerlies across the equator in the east (Philander and Pacanowski, 1981) and enhanced easterlies further to the west (Mitchell and Wallace, 1992; Okumura and Xie, 2004). The low SST and the cross-equatorial southerlies prevent the migration of the ITCZ into the southern hemisphere. Positive ocean–atmosphere feedbacks tend to maintain the cold tongue and the northerly position of the ITCZ (Mitchell and Wallace, 1992; Chang and Philander, 1994; Okumura and Xie, 2004; Xie, 2004, and references therein).

The aim of this study is to examine the ability of fully coupled GCMs to simulate BLs in the tropical Atlantic and to assess the extent to which SST biases can be attributed to errors in the simulated BLs. The paper is organized as follows. Section 2 gives an overview of the models and data used in this study. Section 3 is concerned with the definition of a BL. The BL characteristics of the models are presented in Section 4. The mechanisms behind spurious model BLs in the SeEA are further discussed in Section 5. Section 6 is dedicated to model biases in the SST and the surface wind stress. In Section 7 the contribution of BLs to SST biases is explored. This is followed by a discussion in Section 8. Finally, the main conclusions are given in Section 9.

2. Models and data

Table 1 lists the fully coupled GCMs that are analysed in the present study. The models are selected, based on the availability of subsurface ocean data, from the list of coupled GCMs used for the fourth assessment report of the Intergovernmental Panel on Climate Change (IPCC, 2007). For the analysis we made use of monthly mean model output of the period 1900–1930 of the 20th-century climate (20c3m) scenario simulations.

To assess model biases in the thickness of BLs and in the magnitude of temperature inversions inside BLs, we make use of the observational dataset de Boyer Montégut et al. (2007) derived from the NODC, WOCE and ARGO databases of measured salinity and temperature profiles. Biases in the vertical ocean temperature and salinity stratifications are assessed with help of the 1972–2001 period of the Simple Ocean Data Assimilation (SODA) reanalysis (version 1.4.2; Carton and Giese, 2008). Biases in SST and surface wind stress are computed as the differences in reference to the ERA-40 reanalysis for 1958–2001. Rainfall biases are computed with respect to the CMAP precipitation data (Xie and Arkin, 1997) for 1979–2005 provided by NOAA/OAR/ESRL PSD, Boulder, Colorado, USA, from their web site at http://www.cdc.noaa.gov/.

3. Definition of BLs

Following de Boyer Montégut et al. (2004, 2007) we define the top of the thermocline, or equivalently the isothermal layer depth (ILD), as the depth where the potential temperature has

Table 1. Coupled ocean–atmosphere models considered in this study, with the run number of the 20th-century climate (20c3m) scenario between brackets. The ocean resolution is given along the equator

Model (run #)	period	Res. Atm.	Res. Ocean	Reference
CNRM-CM3 (1)	1900–1929	T63L45	$2^\circ \times 0.5^\circ$ L31	(Salas-Mélia et al., 2005)
CSIRO-Mk3.0 (2)	1901–1930	T63L18	$1.875^\circ \times 0.84^\circ$ L31	(Gordon et al., 2002)
UKMO-HadCM3 (2)	1900–1924	$3.75^\circ \times 2.5^\circ$ L19	$1.25^\circ \times 1.25^\circ$ L20	(Gordon et al., 2000)

dropped by 0.2°C with respect to its value at 10 m. We remark that some other authors define the ILD by a change (±) rather than a drop in temperature (e.g. Kara et al., 2000), but we prefer here to base it on a drop in temperature in order to capture possible subsurface temperature inversions. Similarly, the top of the pycnocline, which corresponds to the mixed-layer depth (MLD), is defined as the depth where the potential density has increased with respect to its value at 10 m by an amount that corresponds to a drop in potential temperature by 0.2°C. In mathematical form, the above definitions can be expressed as:

$$\theta_{z=-\mathrm{ILD}} \equiv \theta_{10\mathrm{m}} - 0.2, \quad (1)$$

$$\sigma_{z=-\mathrm{MLD}} \equiv \sigma(S_{10\mathrm{m}}, \theta_{10\mathrm{m}} - 0.2), \quad (2)$$

where θ is the potential temperature, S is the salinity, and σ is the potential density. In this study the potential density is computed from the 1980 UNESCO International Equation of State (IES80; Gill, 1982). The reference depth of 10 m is based on avoiding the diurnal variability in the vertical stratification in the top few meters just below the ocean surface (de Boyer Montégut et al., 2004, 2007). This reference depth corresponds also with the typical vertical grid resolution near ocean surface in the models. Note that the above definitions imply that the ILD and MLD are at least 10 m thick.

Over most of the tropical Atlantic the pycnocline coincides with the thermocline. An example of this is illustrated in Fig. 1a, which shows the vertical stratification of density, salinity and potential temperature at (30°W, 25°N) in January 1978 according to SODA. Within the mixed layer, which is approximately 70 m thick at this site and time, the profiles are uniform. Just below the mixed layer, the temperature rapidly decreases, while the density increases with depth.

Figure 1b shows the stratification at a different site (50°W, 15°N) in the same month. At this location the vertical salinity stratification is much stronger than at (30°W, 25°N). As a consequence, the mixed layer is about 2.5 times shallower than the isothermal layer. A 40 m thick BL exists between the bottom of the isothermal layer and the mixed layer. The strong salinity stratification even enables a stable density stratification with a temperature inversion inside the BL, that is, the maximum temperature occurs below the mixed layer and it is about 0.3°C higher than the temperature within the mixed layer. Note that when this occurs, entrainment and vertical turbulent mixing at the base of the mixed layer tend to warm the mixed layer contrary to a cooling tendency in the case shown in Fig. 1a.

The strong salinity stratification in Fig. 1b traps the net surface cooling during boreal fall and winter in the mixed layer. Simultaneously, a part of the surface solar radiation penetrates below the mixed layer and tends to heat up the BL (Vialard and Delecluse, 1998a; Masson and Delecluse, 2001). These processes may explain the existence of the temperature inversion in Fig. 1b.

4. BL characteristics

In this section some BL characteristics of the models are shown for boreal winter and summer. The detailed procedure for computing these characteristics is given in the Appendix. The model results are compared against the observational results of de Boyer Montégut et al. (2007). Their computational procedure is somewhat different from ours (see Appendix), but we believe that the differences in the computational procedures are small enough to allow for a direct comparison between the models and the observations.

This section also presents BL characteristics computed from the SODA reanalysis in order to assess how well the reanalysis compares with the observations. This serves to justify the use of the SODA reanalysis as a reference dataset to compute model biases in the upper ocean hydrological structure in the next sections.

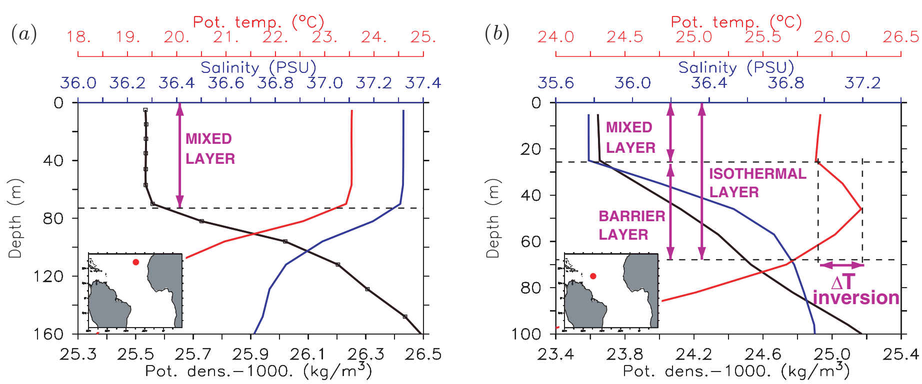

Fig. 1. Examples of vertical stratifications in the tropical Atlantic ocean (a) without and (b) with a BL. The profiles were taken from SODA, January 1978, at the location of the red dot in the insert (30°W,25°N and 50°W,15°N, respectively). The black, red and blue lines depict, respectively, the potential density (in kg m^{-3}), the potential temperature (in°C), and the salinity (in PSU). The square symbols indicate the vertical grid resolution of the data.

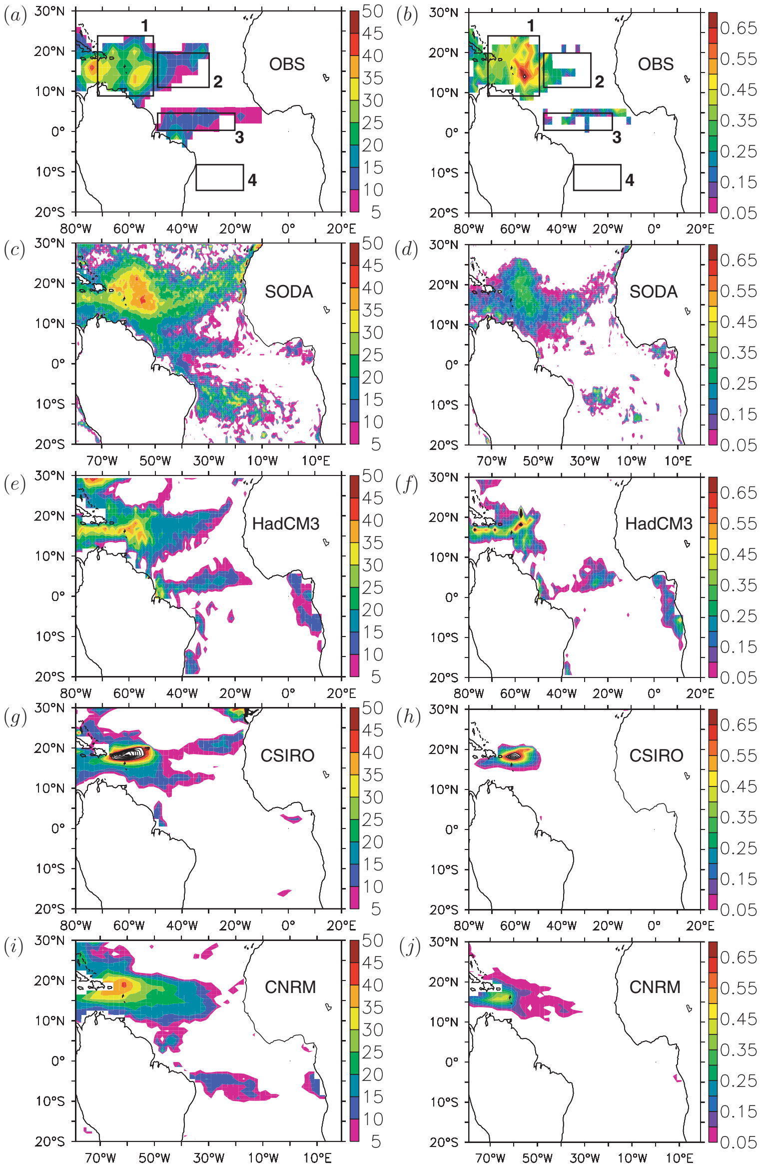

Fig. 2. BL characteristics averaged over boreal winter (DJF), computed from observations by de Boyer Montégut et al. (2007) (top row) and for SODA and the models (other rows). Left panels depict the BL thickness (in m), right panels the magnitude of maximum temperature inversion (in°C). Values beyond the range of the colorkey are contoured; the contour interval is equal to the colour interval. (a)–(b) Observations. (c)–(d) SODA. (e)–(f) UKMO-HadCM3. (g)–(h) CSIRO-Mk3.0. (i)–(j) CNRM-CM3.

4.1. Boreal winter

Figure 2 presents the BL thickness and the magnitude of maximum temperature inversion for boreal winter. The top row depicts the observational results from de Boyer Montégut et al. (2007) and the other rows the results from SODA and the models.

The observational results for the BL thickness (Fig. 2a) show a vast area of thick BLs of up to ∼40 m in the NwTA (box 1), BLs equatorward of the northern subtropical salinity maximum (box 2), and thinner BLs of up to ∼15 m stretched across the width of the Atlantic basin near 5°N (box 3). The BL thickness in SODA (Fig. 2c) agrees fairly well with the observations, although SODA exhibits occasionally present BLs equatorward of the southern subtropical salinity maximum around ∼10°S (box 4) and directly off the coast of Northwest Africa near 20°N that are absent in the observations.

The UKMO-HadCM3 model (Fig. 2e) reproduces the observational results for the BL thickness remarkably well, while the CSIRO-Mk3.0 and the CNRM-CM3 models position the thickest BLs a bit too far to the north and fail to simulate the equatorial BL region near 5°N. Furthermore, the CSIRO-Mk3.0 model displays a small region centred around ∼(60°W, 18°N) where the BLs are excessively thick (Fig. 2g).

In the observations the thick BLs in the NwTA (box 1) are associated with strong maximum temperature inversions of up to 0.7°C (Fig. 2b). The models generally underestimate the magnitude of the maximum temperature inversions with the notable exception of the region around ∼(60°W, 18°N) in the CSIRO-Mk3.0 model where temperature inversions are far too strong (Fig. 2h).

The thick BLs in the NwTA (box 1) are very robust, with a frequency of occurrence of near 100% in SODA (i.e. these BLs show up every winter). In agreement with SODA, the models show also a robust presence of BLs in the NwTA (not shown).

As mentioned in the introduction, the thick BLs with temperature inversions in the NwTA are believed to originate primarily from advection of fresh Amazon water by surface ocean currents in combination with surface cooling during boreal fall and winter (Mignot et al., 2007). This mechanism seems to be consistent with the Sea Surface Salinity (SSS) field of SODA (not shown), which clearly shows a low salinity plume extending from the mouth of the Amazon river (∼50°W, 0°N) along the northern coast of South America towards the east of the Caribbean basin. A similar plume is clearly visible in the BL characteristics of SODA (Figs. 2c and d). The BL characteristics of the models and the observations exhibit also plume-like features, although less pronounced compared to SODA.

4.2. Boreal summer

The models and SODA capture the reduction in the regional extent and thickness of the BLs in the NwTA (box 1), which is presumably the result of summer warming and a reduction in wind-induced mixing (Mignot et al., 2007). But along the northern coast of South America just south of this BL region, the UKMO-HadCM3 and CNRM-CM3 models display excessively thick BLs, which in the UKMO-HadCM3 model are accompanied by strong temperature inversions as well (Fig. 3f). Unlike the observations, the UKMO-HadCM3 and CNRM-CM3

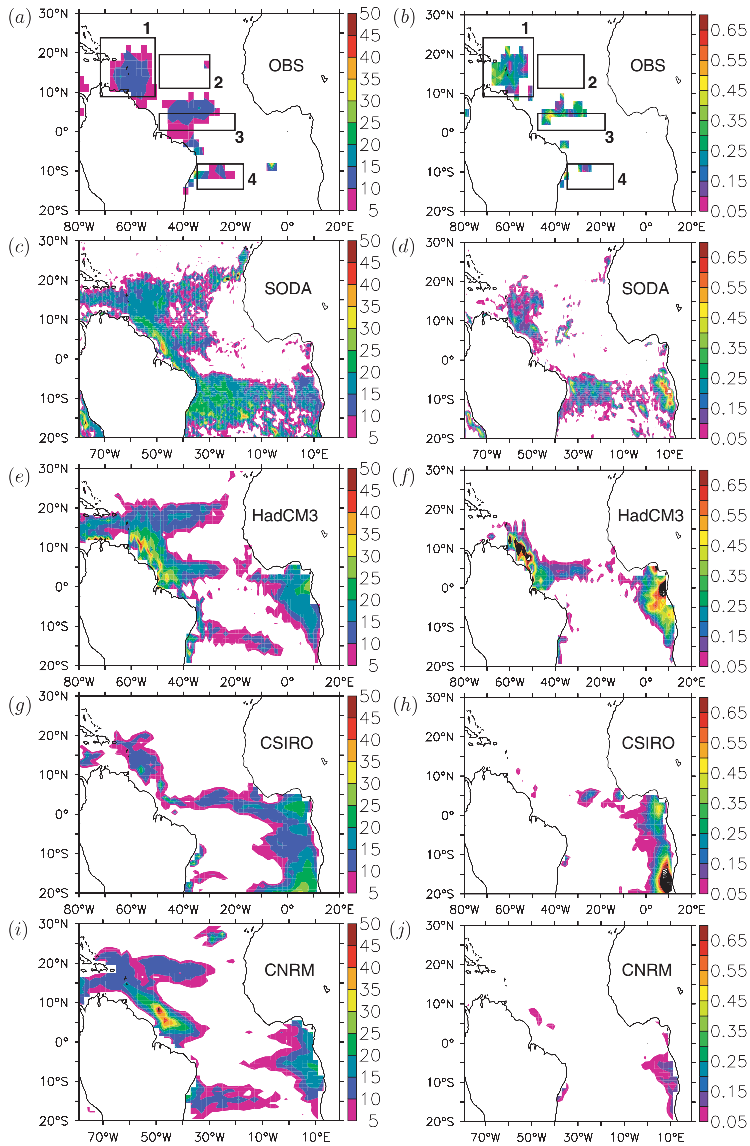

Fig. 3. Same as Fig. 2, but now for boreal summer (JJA).

models still simulate the presence of BLs equatorward of the northern subtropical salinity maximum (box 2). Furthermore, they capture the BLs equatorward of the southern subtropical salinity maximum (box 3), but the extent of this BL region is too large and positioned a bit too far to the south.

All models simulate an equatorial BL region around $\sim$5°N, although the thickness of these BLs varies considerably among the models. In reality the fresh surface water of this BL region originates partly from the Amazon river, which feeds the North Brazil Current (NBC). A part of the water from the NBC flows into the NBC retroflection and is advected eastward by the NECC along $\sim$6°N during boreal summer and fall (e.g. Pailler et al., 1999; Mignot et al., 2007). This mechanism is likely to play an important role in the formation of these BLs in the UKMO-HadCM3 model, as Figs. 3e and f show a clear plume structure that extends from the mouth of the Amazon river towards the north along the western boundary and eastward along the NECC. Intense local precipitation associated with the overlying ITCZ may also have contributed to the formation of the BLs (Foltz et al., 2004; Mignot et al., 2007).

A striking difference between the models and the observations is the presence of spurious BLs in the SeEA along the African coast in the models. These spurious BLs also show up in SODA, but in SODA they are much less robust than in the models where the frequency of BL occurrence locally displays values of up to 100% (not shown). The thickness of these model BLs is typically in the range of 10–20 m. Temperature inversions also display very high values, with maxima larger than 1°C for the UKMO-HadCM3 and the CSIRO-Mk3.0 model. Interestingly, this BL region coincides with the ACT region where the models show a strong warm SST bias as discussed in the introduction. The mechanisms behind the presence of this BL region in the models will be discussed in the next section.

5. Mechanisms of spurious model BLs in the SeEA

Figure 4 presents the seasonal variation of the vertical stratification in salinity and temperature horizontally averaged over the ACT region. The latter is defined here as the region extending from 10°W to 10°E and 5°S to 0°N. The solid and dashed lines depict the seasonal cycle of the MLD and the ILD, respectively. In SODA, the MLD closely follows the ILD throughout the year, indicating that the vertical stratification in density is mainly controlled by the temperature. Indeed, the seasonal variation in the salinity stratification is weak, while it is strong in the temperature stratification (Figs. 4a and b). The SST varies from near 29°C in March to 23.5°C in August. Similarly, the MLD and ILD vary between roughly 15 m in March and 20 m in October.

In contrast to SODA, for all three models the ILD is significantly larger than the MLD during boreal spring and summer. This indicates the presence of a BL in these seasons and hints at the important role of salinity in determining the vertical density stratification. In all models the isothermal layer deepens strongly from 15 to 20 m in boreal spring to about 30 m in early summer, while the variation in MLD is much weaker. In the UKMO-HadCM3 model the MLD remains nearly unchanged. The BL formation in the models, as revealed by Fig. 4, results from the combined effect of very fresh water at the surface and the development of a warm subsurface bias from spring to summer. These erroneous features are especially pronounced for the UKMO-HadCM3 model where the error in SSS is as large as 3 PSU (Fig. 4c) and the error in temperature is near 8°C at 45–65 m depth in June (Fig. 4d).

The origin of the warm bias in the subsurface temperature will be discussed in the following section. Here we note that the temperature bias patterns of the models are tilted upward in the depth–time plots shown in Fig. 4, indicating that the subsurface temperature errors are 'propagating' upward into the mixed layer. While in SODA the upwelling of cold subsurface water in boreal spring and summer causes rapid cooling of the surface and the development of the ACT, in the models the warm subsurface bias substantially reduces the surface cooling. This likely explains the upward propagation of temperature biases.

Different from the temperature bias patterns, the salinity bias patterns of the models do not show an upward tilt, suggesting that the fresh salinity bias at the surface is a consequence of horizontal advection by the surface currents and/or a local E-P surface flux error rather than related to subsurface processes. Figure 5 shows the model precipitation biases in the tropical Atlantic during JJA in reference to the CMAP observational dataset. The observations show that the position of the marine ITCZ is centred around the latitude band of 6–8°N. In the models the marine ITCZ is shifted towards the southeast, causing a negative precipitation bias to the north and a positive precipitation bias in and south of the ACT region. This suggests that the low SSS in the ACT region is caused by excessive rainfall. A budget analysis of the mixed-layer salinity confirmed that this is the primary cause of the low SSS, but also indicated an important contribution from meridional transport of fresh water by the surface currents (not shown). It is noted, however, that the latter contribution may actually be related to excessive precipitation as well, since Fig. 5 shows that the precipitation bias pattern extends also over the region south of the ACT region.

6. SST and wind stress biases

In this section we discuss the model biases in SST and wind stress over the tropical Atlantic. The biases for DJF and JJA are depicted in Fig. 6. Note that for all models the SST bias patterns look fairly similar, which suggests that the SST biases may be caused by common physical processes. Cold SST biases are observed over the western equatorial Atlantic and further poleward of the equator. The wind stress bias of the CNRM-CM3 model (Figs. 6c and f) shows that the trade wind over the northern tropical Atlantic is far too strong, suggesting that the strong cold

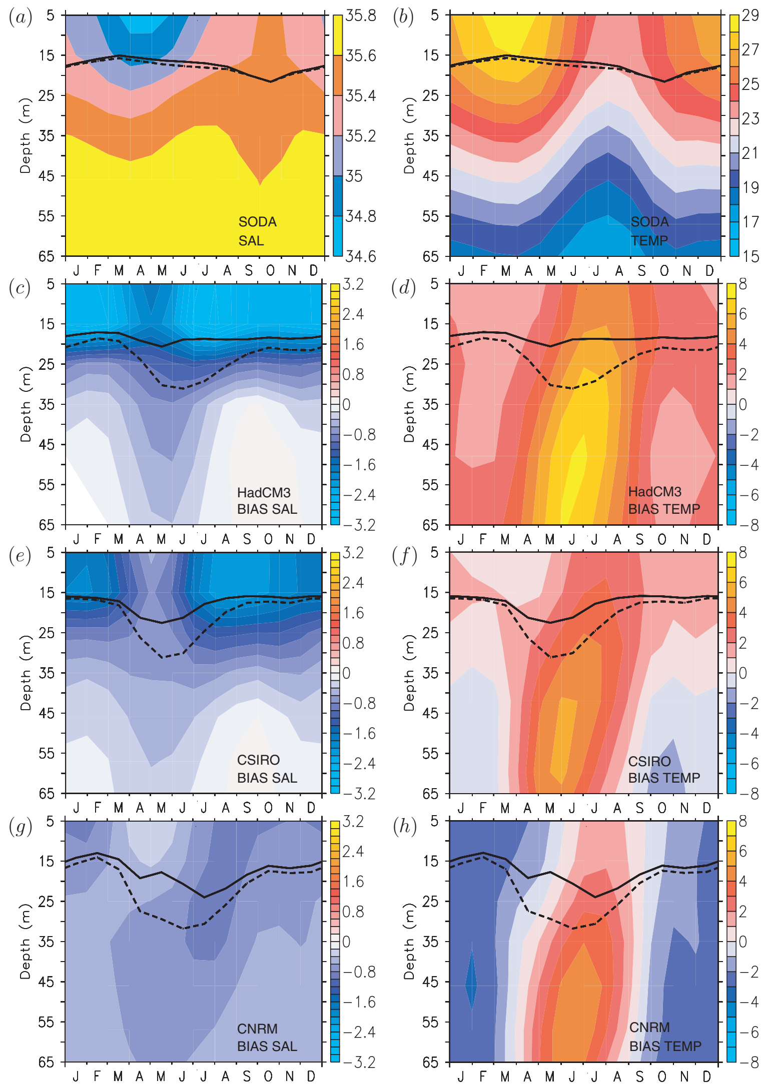

Fig. 4. Vertical stratification in salinity (left panels, in PSU) and potential temperature (right panels, in°C) averaged over the ACT region from 10°W to 10°E and 5°S to 0°N. The solid and dashed lines depict, respectively, the mixed–layer depth and the isothermal layer depth. (a, b) SODA. (c, d) Biases UKMO-HadCM3 model. (e, f) Biases CSIRO-Mk3.0 model. (g, h) Biases CNRM-CM3 model.

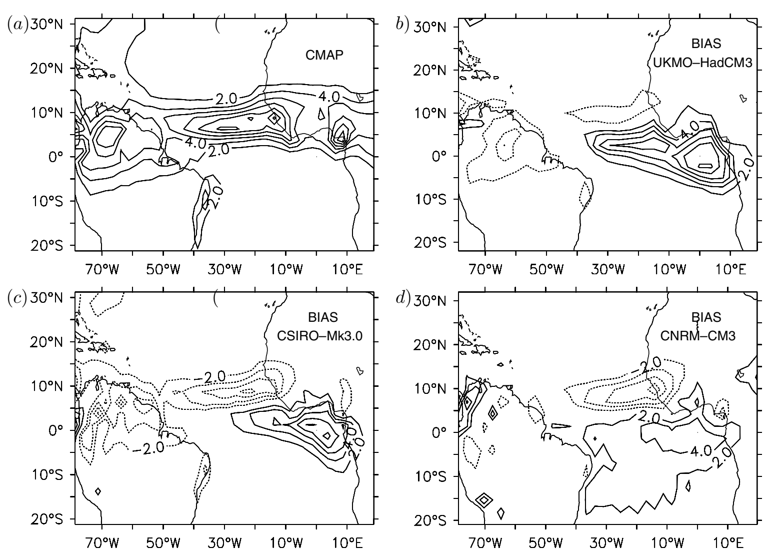

Fig. 5. Rainfall in the tropical Atlantic during JJA (contour interval of 2 mm d^{-1}). (a) CMAP observations. (b) Bias UKMO-HadCM3 model. (c) Bias CSIRO-Mk3.0 model. (d) Bias CNRM-CM3 model.

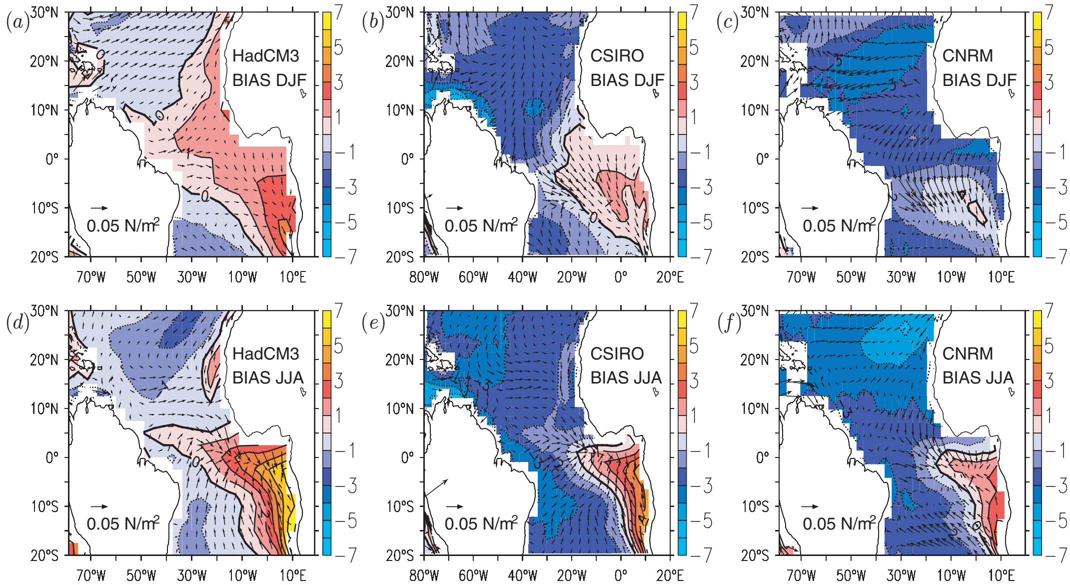

Fig. 6. Model biases in SST and surface wind stress during DJF (top panels) and JJA (bottom panels) with respect to the ERA-40 reanalysis. (a, d) Biases UKMO-HadCM3 model. (b, e) Biases CSIRO-Mk3.0 model. (c, f) Biases CNRM-CM3 model.

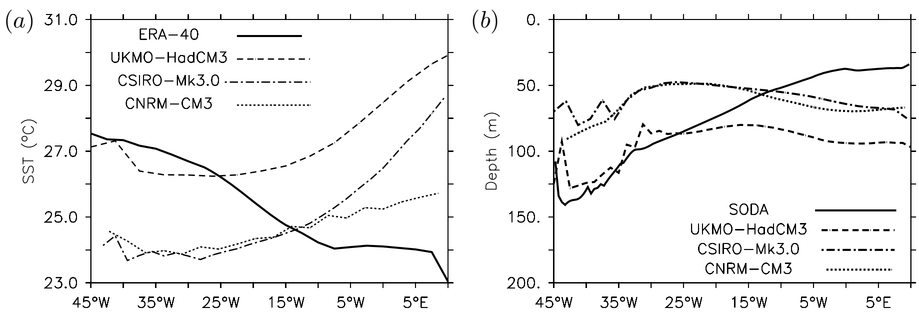

Fig. 7. (a) Boreal summer (JJA) SST along the equator and averaged between 5°S and 0°N. Solid line represents the ERA-40 SST, while the other lines depict the SST for the models. (b) Same as (a), but now for the depth of the 20°C-isotherm, which is a proxy for the depth of the equatorial thermocline.

SST bias of more than 3°C in this area may originate largely from excessive latent cooling. In contrast, the northeasterly trade wind is too weak in the UKMO-HadCM3 model, but this model still has a cold SST bias in this region, albeit weaker compared to the CNRM-CM3 model. This suggests that other physical processes also contribute to the cold bias.

In all the models warm SST biases are observed over the SeEA in boreal summer, particularly in the UKMO-HadCM3 model with biases exceeding 5°C over the ACT region. As a consequence, the zonal SST gradient along the equator is directed towards the east in the models instead of towards the west in reality as depicted in Fig. 7a. Consistent with the wrong zonal SST gradient and the attendant bias in the zonal surface pressure gradient (not shown), there is a strong westerly wind stress bias in the equatorial trade. The westerly wind stress bias affects the depth of the thermocline as shown in Fig. 7b. In the SODA reanalysis the thermocline is deeper than 125 m in the western equatorial Atlantic and shoals eastward to about 35 m. In the models, however, the thermocline is too shallow in the west, but too deep in the east, and it reaches a minimum depth around 35–15°W.

The westerly wind stress bias and the associated thermocline bias over the eastern equatorial Atlantic, explain the strong warm subsurface temperature bias during spring and summer in Figs. 4d,f and h. Furthermore, the cold SST bias over the northern tropical Atlantic and the strong warm SST bias over the SeEA are consistent with the southeastward displacement of the marine ITCZ in the models (Fig. 5), as deep convection tends to be collocated with the maxima in SST. One may therefore tend to attribute the fresh SSS bias over the SeEA to the warm SST bias. However, cause and effect are difficult to separate here, because the fresh SSS bias together with the warm subsurface temperature bias gives rise to spurious BLs during boreal spring and summer (Fig. 4), which in turn affects the SST by suppressing entrainment and turbulent mixing of cold subsurface water into the mixed layer.

7. Contribution of BLs to SST biases

In this section we explore the contribution of model biases in the representation of BLs to biases in the SST in the tropical Atlantic. We focus on two BL regions. The first region is the NwTA characterized by a vast area of thick BLs with temperature inversions during boreal winter. The models capture this BL region, though they generally underestimate the magnitude of the maximum temperature inversion (Fig. 2). The second region is the ACT region, where the models develop spurious BLs with strong temperature inversions during boreal spring and summer (Figs. 3 and 4). It may be expected that the BL biases contribute to the biases in the SST, since BLs affect the turbulent mixing and entrainment of cold subsurface water into the mixed layer.

Unfortunately, it is very difficult to assess the vertical turbulent mixing and entrainment heat flux in the models, since these processes are parametrized and a reconstruction based on available monthly mean model output would be inaccurate. However, what can be assessed is the temperature difference between the core and the base of the mixed layer, $\langle T \rangle - T|_{-h}$, where $\langle T \rangle = (1/h) \int_{-h}^{0} T \, dz$. The vertical turbulent mixing and entrainment heat flux both scale with this temperature difference (Kraus and Turner, 1967; Stevenson and Niiler, 1983). Biases in the representation of BLs will affect this temperature difference, and thus the vertical heat flux at the base of the mixed layer and consequently the SST.

Figure 8a depicts the temperature difference between core and base of the mixed-layer in the NwTA, loosely defined here as the region extending from 65°W to 45°W and 10°N to 25°N. Compared to SODA, the models overestimate the temperature difference over the period Nov.-Feb., while, to a lesser extent, they underestimate it during the period Apr.-Sep. On yearly average, the bias in the temperature difference is small. Furthermore, the observational study by Foltz et al. (2003) showed that in the northern central tropical Atlantic (directly east of the NwTA), the mixed-layer heat budget is dominated by the surface heat fluxes and the heat storage rate. In the models the same terms also appear to be in approximate balance in the NwTA. This indicates that the vertical turbulent mixing and entrainment heat flux play only a minor role in the mixed-layer heat budget in the NwTA. It is therefore likely that the contribution from BL biases to the cold SST bias in this region is small.

Figure 8b shows the temperature difference between core and base of the mixed-layer in the ACT region. Relative to SODA, the models strongly underestimate the temperature difference, in particular during boreal spring and summer, when the bias may be larger than 0.25°C. This is consistent with the presence of spurious BLs in this region during these seasons (Figs. 3 and 4). Different from the NwTA, in the ACT region entrainment and vertical turbulent mixing are very important, as they are responsible for the rapid development of the equatorial Atlantic cold tongue in late boreal spring and summer (Foltz et al., 2003; Jochum et al., 2005; Peter et al., 2006). This suggests that the spurious BLs contribute significantly to the warm SST bias in this region in the models.

8. Potential coupled feedback mechanism

The analysis presented in the previous section suggests that the model errors in simulating BLs have a significant impact on SST biases in the SeEA, while their impact is relatively small in the NwTA. However, this assessment may be incomplete because it does not fully take into account the effect of coupled ocean–atmosphere feedbacks. The tropical Atlantic is an area where ocean–atmosphere interactions are known to be strong. Because of the active air–sea coupling, small model errors in one physical process can cause chain reactions and affect other physical processes. For example, BL biases can cause SST biases which in turn can affect atmospheric convection, introducing errors in surface heat fluxes and other physical processes. This makes it very difficult to pinpoint exactly how much of the model SST biases can be attributed to BL biases. Therefore, further understanding of the impact of BLs on SST

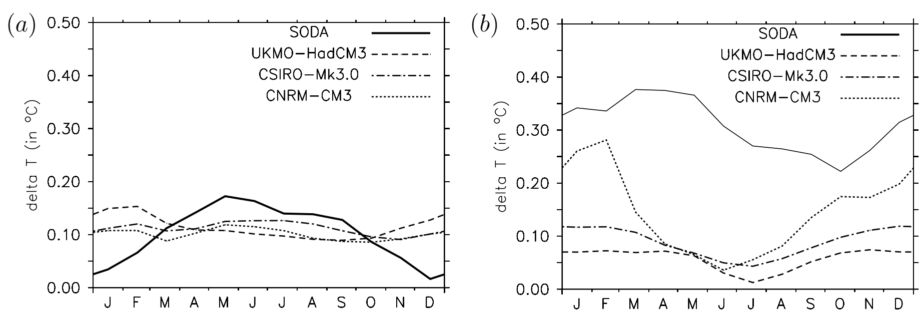

Fig. 8. (a) Temperature difference between core and base of the mixed layer, $\langle T \rangle - T|_{-h}$, averaged over the NwTA (in °C). (b) Same as (a), but now for the ACT region.

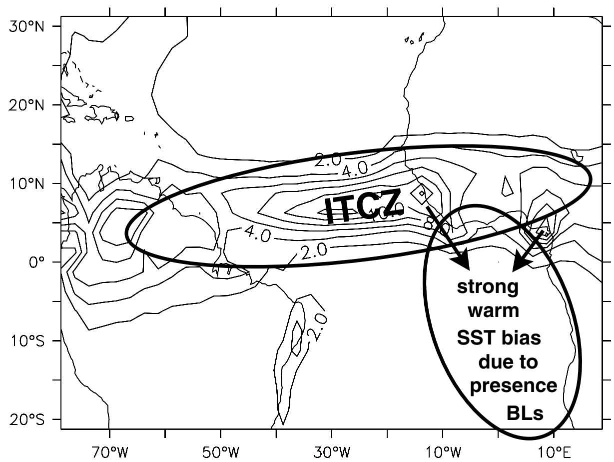

Fig. 9. Illustration of a potential feedback mechanism between BLs, SST and ITCZ in the SeEA. Background contours show the precipitation during JJA (in mm d^{-1}) from CMAP observations. The arrows indicate the southeastward displacement of the ITCZ in the models.

requires the understanding of coupled feedbacks in the climate system.

Based on this study we hypothesize that the SeEA is one of the regions in the tropical Atlantic where BL and SST biases may amplify each other. A potential positive BL–SST–ITCZ feedback mechanism is illustrated in Fig. 9. In the SeEA the models simulate spurious BLs with strong temperature inversions during boreal spring and summer. This prevents cooling of the mixed layer by vertical turbulent mixing and entrainment, as indicated by the results in previous sections. As a result, a warm SST bias develops, which keeps the ITCZ closer to the equator. The displaced ITCZ is responsible for excessive precipitation over the SeEA, which creates a layer of fresh surface water. Meanwhile, the warm SST bias over the SeEA weakens the equatorial easterlies, resulting in a deepened thermocline in the east and subsurface warming. The combined effect of freshening at the surface and warming at the subsurface maintains the spurious BLs and thus the warm SST bias.

Previous studies proposed several other causes for the strong warm SST bias over the SeEA. DeWitt (2005) suggested that it originates primarily from the too weak equatorial trade winds. This causes a too deep thermocline and too weak upwelling in the east, that both contribute to a reduction in entrainment cooling, while the opposite holds for the western equatorial Atlantic. A similar explanation was given by Chang et al. (2007) for the warm SST bias in the ACT region in the NCAR-CCSM3 model (Collins et al., 2006). As mentioned earlier, because of the tight air–sea coupling in the trade-wind-cold-tongue system, cause and effect of the weak trade wind and warm SST biases are difficult to assess. Hazeleger and Haarsma (2005) demonstrated the sensitivity of the cold tongue SST to changes in the wind-induced vertical mixing scheme for the upper ocean. Increasing the efficiency of vertical mixing led to a reduction in the warm SST bias over the cold tongue region in their coupled model and improved the seasonal migration of the marine ITCZ. All these studies suggest that a Bjerknes-type of feedback (Bjerknes, 1969) between SST, equatorial easterlies and thermocline displacement plays an important role in maintaining the warm SST bias over the SeEA in coupled climate models. The results presented in Section 6 seem to confirm that this mechanism is at work, but our study suggests furthermore that it operates in concert with other mechanisms, such as the BL–SST–ITCZ feedback mechanism. Targeted sensitivity simulations with coupled models are needed to further test and quantify the importance of these feedback mechanisms.

The misrepresentation of the feedback between marine stratus clouds and local SST (Philander et al., 1996) has also been proposed as a possible cause for the warm SST bias off the African coast in the South Atlantic. The BL–SST–ITCZ feedback possibly enhances the stratus-SST feedback in this area, as some models, such as CSIRO-Mk3.0 model, develop a BL with a strong temperature inversion along the African coast during boreal summer (Fig. 3).

9. Conclusions

The investigated coupled climate models capture the major observed BL regions in the tropical Atlantic, although with considerable biases in the characteristics of the BLs. The models are capable of simulating thick and robust BLs in the NwTA during boreal winter, but they generally underestimate the magnitude of the subsurface temperature inversion in this BL region. The present results indicate that the effect of BL biases in the NwTA on the cold SST bias in this region is likely small, since the annually averaged bias in the temperature difference between the core and base of the mixed layer is small and vertical turbulent mixing and entrainment are only minor terms in the mixed-layer heat budget.

Contrary to observations, the models generate spurious BLs over the SeEA during boreal spring and summer. These BLs tend to suppress the development of the Atlantic cold tongue in these seasons, and seem to contribute significantly to the warm SST bias in this area. The formation of these BLs likely originates from the low SSS year round and the development of a warm subsurface bias during boreal spring and summer. The low SSS is caused by excessive precipitation over the ACT region associated with the southeastward displaced ITCZ during boreal spring and summer. The warm subsurface bias is probably caused by the too weak equatorial trades, making the thermocline too shallow in the west and too deep in the east.

We hypothesized that a positive BL–SST–ITCZ feedback mechanism exists that tends to maintain the BL and SST biases in the SeEA. According to this hypothesis, the spurious presence of BLs causes a warm SST bias. The warm SST bias results in a warm subsurface bias through a weakening of the equatorial easterlies and the attendant change in the tilt of the equatorial thermocline. The warm SST bias also keeps the ITCZ close to the equator, resulting in excessive precipitation and a fresh surface layer in the SeEA. The combined effect of a warm subsurface bias and a fresh surface bias maintains the presence of the BLs and thus the warm SST bias in this region.

This study shows that the upper ocean salinity stratification plays an important role in the chain of cause and effect of biases in coupled models. Furthermore, the BL–SST–ITCZ feedback mechanism implies that precipitation and wind stress biases already present in uncoupled atmospheric models (Biasutti et al., 2006) are amplified in coupled models. Amplification of biases would occur even in the ideal case when coupled models perfectly capture the ocean physics and the coupled climate feedbacks. This suggests that coupled model biases originate largely from the atmosphere. Therefore, it is expected that most improvement of coupled models can be obtained when modellers focus on improvement of key atmospheric processes such as precipitation.

10. Acknowledgments

We acknowledge the international modelling groups for providing their data for analysis, the Program for Climate Model Diagnosis and Intercomparison (PCMDI) for collecting and archiving the model data, the JSC/CLIVAR Working Group on Coupled Modelling (WGCM) and their Coupled Model Intercomparison Project (CMIP) and Climate Simulation Panel for organizing the model data analysis activity, and the IPCC WG1 TSU for technical support. The IPCC Data Archive at Lawrence Livermore National Laboratory is supported by the Office of Science, U.S. Department of Energy. The figures in this paper have been made with the free Ferret software developed by TMAP at NOAA/PMEL. WPB acknowledges the Netherlands Organization for Scientific Research (NWO) for financial support under the ALW-project 854.00.014. PC would like to acknowledge the supports from the National Science Foundation through grant ATM-0337846 and OCE-0623364 and from the National Oceanic and Atmospheric Administration (NOAA)'s Climate Program grant through NA050AR4311136.

11. APPENDIX A: Procedure for computing BL characteristics

For each month and at each gridpoint of the model output, the ILD and the MLD were computed based on the criteria given by eqs (1) and (2), respectively. If the ILD exceeded the MLD by 10 m, then the layer in between the base of the ILD and MLD was considered as a 'true' BL, and its thickness was computed as the difference ILD–MLD. A threshold of 10 m was chosen, because in the models this corresponds to the typical vertical grid resolution near ocean surface. When a true BL was detected, it was checked whether the vertical temperature profile contained a subsurface maximum inside the BL, and if so, the magnitude of the maximum temperature inversion was computed as the difference between the maximum temperature and the temperature at 10 m depth. Next, the monthly climatologies were computed by averaging over all years in which a BL was detected. For example, the climatological mean BL thickness for January was computed by averaging over all years in which a BL was detected in January.

The seasonal climatologies shown in Figs. 2 and 3 were obtained by averaging the monthly climatologies over the respective seasons. Because at some gridpoints a BL may be detected in a specific month, but possibly never in the preceding and/or the next month, the gridpoints of the monthly climatology fields without a value (i.e. where a BL was never detected) were first assigned the value 0 prior to the seasonal averaging.

In Figs. 2 and 3 the model and SODA results for the BL thickness and the magnitude of the temperature inversion are compared against the observational results of de Boyer Montégut et al. (2007). Inherent to the differences between the model and the observational datasets, the computational procedure of de Boyer Montégut et al. (2007) deviates from our procedure. The main differences are:

(1) They computed the BL characteristics from instantaneous stratification profiles and did the monthly averaging afterward, whereas we computed the BL characteristics from monthly mean stratification profiles.

(2) They grouped their data in $2^\circ \times 2^\circ$ grid boxes, then took the median of the BL characteristics within these grid boxes and applied a weak spatial smoothing to reduce noise. We computed our BL characteristics directly at every model gridpoint without any spatial smoothing.

(3) They did not use a threshold of 10 m to define a 'true' BL. Furthermore, they did not require that the difference ILD–MLD should be positive.

It is difficult to quantify the effect of the differences in the computational procedures on the model biases in BL characteristics. In the present study we simply assume that this effect is small.

Similar as we did for the models and SODA, the seasonal climatologies of the observations were obtained by averaging the monthly climatologies over the respective seasons. Prior to seasonal averaging, negative values of the difference ILD–MLD were put to zero. In the plots of the magnitude of the temperature inversion (Figs. 2b and 3b), those grid points with a seasonal BL thickness of less than 5 m were masked out.

References

Biasutti, M., Sobel, A. H. and Kushnir, Y. 2006. AGCM precipitation biases in the tropical Atlantic. *J. Clim.* **19**, 935–958.

Bjerknes, J. 1969. Atmospheric teleconnections from the equatorial Pacific. *Mon. Wea. Rev.* **97**(3), 163–172.

Breugem, W.-P., Hazeleger, W. and Haarsma, R. J. 2006. Multimodel study of tropical Atlantic variability and change. *Geophys. Res. Lett.* **33**, L23706, doi:10.1029/2006GL027831.

Carton, J. A. and Giese, B. S. 2008. A reanalysis of ocean climate using SODA. *Mon. Wea. Rev.*, in press.

Chang, P. and Philander, S. G. 1994. A coupled ocean-atmosphere instability of relevance to the seasonal cycle. *J. Atmos. Sci.* **51**, 3627–3648.

Chang, C.-Y., Carton, J. A., Grodsky, S. A. and Nigam, S. 2007. Seasonal Climate of the Tropical Atlantic Sector in the NCAR Community Climate System Model 3: error Structure and Probable Causes of Errors. *J. Clim.* **20**(6), 1053–1070.

Collins, W. D., Blackmon, M. L., Bonan, G. B., Hack, J. J., Henderson, T. B. and co-authors. 2006. The Community Climate System Model version 3 (CCSM3). *J. Clim.* **19**(11), 2122–2143.

Davey, M. K., Huddleston, M., Sperber, K. R., Braconnot, P., Bryan, F. and co-authors. 2002. STOIC: a study of coupled model climatology and variability in tropical ocean regions. *Clim. Dyn.* **18**, 403–420.

de Boyer Montégut, C., Madec, G., Fischer, A. S., Lazar, A. and Iudicone, D. 2004. Mixed layer depth over the global ocean: An examination of profile data and a profile-based climatology. *J. Geophys. Res.* **109**, C12003, doi:10.1029/2004JC002378.

de Boyer Montégut, C., Mignot, J., Lazar, A. and Cravatte, S. 2007. Control of salinity on the mixed layer depth in the world ocean. 1. General description. *J. Geophys. Res.* **112**, C06011, doi:10.1029/2006JC003953.

DeWitt, D. G. 2005. Diagnosis of the tropical Atlantic near-equatorial SST bias in a directly coupled atmosphere-ocean general circulation model. *Geophys. Res. Lett.* **32**, L01703.

Foltz, G. R., Grodsky, S. A. and Carton, J. A. 2003. Seasonal mixed layer heat budget of the tropical Atlantic ocean. *J. Geophys. Res.* **108**(C5), 3146.

Foltz, G. R., Grodsky, S. A. and Carton, J. A. 2004. Seasonal salt budget of the northwestern tropical Atlantic ocean along 38°W. *J. Geophys. Res.* **109**, C03052, doi:10.1029/2003JC002111.

Gill, A. E. 1982. *Atmosphere-Ocean Dynamics.* Academic Press, San Diego, USA, 662 pp.

Godfrey, J. S. and Lindstrom, E. J. 1989. The heat budget of the equatorial western Pacific surface mixed layer. *J. Geophys. Res.* **94**(C6), 8007–8017.

Gordon, C., Cooper, C., Senior, C. A., Banks, H., Gregory, J. M. and co-authors. 2000. The simulation of SST, sea ice extents and ocean heat transports in a version of the Hadley Centre coupled model without flux adjustments. *Clim. Dyn.* **16**, 147–168.

Gordon, H. B., Rotstayn, L. D., McGregor, J. L., Dix, M. R., Kowalczyk, E. A. and co-authors. 2002. The CSIRO Mk3 climate system model. CSIRO Atmos. Res. Tech. Pap. No. 60, 130 pp. CSIRO, Division of Atmospheric Research, Australia.

Hazeleger, W. and Haarsma, R. J. 2005. Sensitivity of tropical Atlantic climate to mixing in a coupled ocean-atmosphere model. *Clim. Dyn.* **25**, 387–399.

IPCC 2007. *Climate change 2007: the physical science basis. Contribution of Working Group I to the fourth assessment report of the Intergovernmental Panel on Climate Change*, (eds S. Solomon, D. Qin, M. Manning, Z. Chen, M. Marquis and co-editors), Cambridge University Press, Cambridge, United Kingdom and New York, NY, USA, 996 pp.

Jochum, M., Murtugudde, R., Ferrari, R. and Malanotte-Rizzoli, P. 2005. The impact of horizontal resolution on the tropical heat budget in an Atlantic ocean model. *J. Clim.* **18**(6), 841–851.

Kara, A. B., Rochford, P. A. and Hurlburt, H. E. 2000. Mixed layer depth variability and barrier layer formation over the North Pacific Ocean. *J. Geophys. Res.* **105**(C7), 16 783–16 801.

Kraus, E. B. and Turner, J. S. 1967. A one-dimensional model of the seasonal thermocline. II: the general theory and its consequences. *Tellus* **19**, 98–105.

Maes, C., Picaut, J. and Belamari, S. 2002. Salinity barrier layer and onset of El Ni no in a Pacific coupled model. *Geophys. Res. Lett.* **29**(24), 59.1–59.4.

Masson, S. and Delecluse, P. 2001. Influence of the Amazon river runoff on the tropical Atlantic. *Phys. Chem. Earth, part B* **26**(2), 137–142.

Mignot, J., de Boyer Montégut, C., Lazar, A. and Cravatte, S. 2007. Control of salinity on the mixed layer depth in the world ocean. 2: tropical areas. *J. Geophys. Res.* **112**, C10010, doi:10.1029/2006JC003954.

Mitchell, T. and Wallace, J. M. 1992. The annual cycle in equatorial convection and sea surface temperature. *J. Clim.* **5**, 1140–1156.

Murtugudde, R. and Busalacchi, A. J. 1998. Salinity effects in a tropical ocean model. *J. Geophys. Res.* **103**(C2), 3283–3300.

Okumura, Y. and Xie, S.-P. 2004. Interaction of the Atlantic equatorial cold tongue and the African monsoon. *J. Clim.* **17**, 3589–3602.

Pailler, K., Bourlès, B. and Gouriou, Y. 1999. The barrier layer in the western tropical Atlantic Ocean. *Geophys. Res. Lett.* **26**(14), 2069–2072.

Peter, A.-C., Le Hénaff, M., Du Penhoat, Y., Menkes, C. E., Marin, F. and co-authors. 2006. *J. Geophys. Res.* **111**, C06014, doi:10.1029/2005JC003157.

Philander, S. G. H. and Pacanowski, R. C. 1981. The oceanic response to cross-equatorial winds (with application to coastal upwelling in low latitudes). *Tellus* **33**, 201–210.

Philander, S. G. H., Gu, D., Lambert, G., Li, T., Halpern, D. and co-authors. 1996. Why the ITCZ is mostly north of the equator. *J. Clim.* **9**(12), 2958–2972.

Salas-Mélia, D., Chauvin, F., Déqué, M., Douville, H., Gueremy, J. F. and co-authors. 2005. Description and validation of the CNRM-CM3 global coupled model. CNRM working note 103, 36 pp. Centre National de Recherches Météorologiques, Météo-France, France.

Sato, K., Suga, T. and Hanawa, K. 2006. Barrier layers in the subtropical gyres of the world's oceans. *Geophys. Res. Lett.* **33**, L08603, doi:10.1029/2005GL025631.

Sprintall, J. and Tomczak, M. 1992. Evidence of the barrier layer in the surface layer of the tropics. *J. Geophys. Res.* **97**(C5), 7305–7316.

Stevenson, J. W. and Niiler, P. P. 1983. Upper ocean heat budget during the Hawaii-to-Tahiti shuttle experiment. *J. Phys. Ocean.* **13**, 1894–1907.

Uppala, S. M., Kallberg, P. W., Simmons, A. J., Andrae, U., Da Costa Bechtold, V. and co-authors. 2005. The ERA-40 reanalysis. *Quart. J. Royal Meteorol. Soc.* **131**(612), 2961–3012.

Vialard, J. and Delecluse, P. 1998a. An OGCM study for the TOGA decade. Part I: role of salinity in the physics of the western Pacific fresh pool. *J. Phys. Ocean.* **28**, 1071–1088.

Vialard, J. and Delecluse, P. 1998b. An OGCM study for the TOGA decade. Part II: barrier-layer formation and variability. *J. Phys. Ocean.* **28**, 1089–1106.

Xie, P. and Arkin, P. A. 1997. Global precipitation: a 17-year monthly analysis based on gauge observations, satellite estimates, and numerical model outputs. *Bull. Amer. Meteor. Soc.* **78**, 2539–2558.

Xie, S.-P. 2004. The shape of continents, air–sea interaction, and the rising branch of the Hadley circulation. In: *The Hadley Circulation: Past, Present and Future*, (eds H. F. Diaz and R. S. Bradley), Kluwer Academic Publishers, Dordrecht, The Netherlands, 121–152.